Quaternary Science Reviews 75 (2013) 11–21

Contents lists available at SciVerse ScienceDirect

Quaternary Science Reviews

journal homepage: www.elsevier.com/locate/quascirev

Reconstructing paleoseismic deformation, 1: modern analogues from the 1960 and 2010 Chilean great earthquakes☆

E. Garrett*, I. Shennan, E.P. Watcham [1], S.A. Woodroffe

Durham University, Sea Level Research Unit, Department of Geography, South Road, Durham DH1 3LE, UK

ARTICLE INFO

Article history:
Received 3 October 2012
Received in revised form
26 March 2013
Accepted 2 April 2013
Available online 21 June 2013

Keywords:
1960 Valdivia earthquake
2010 Maule earthquake
Earthquake reconstruction
Tsunami
Diatoms

ABSTRACT

The 1960, and 2010 Chilean great earthquakes provide modern analogues for the sedimentary signatures of the largest megathrust events and their accompanying tsunamis. This paper presents lithological and diatom assemblage data from five sites and provides key insights for the development of longer earthquake chronologies, essential for assessing the seismic hazards associated with a subduction zone. We find that the 1960 and 2010 tsunami deposits are fragmentary, variable and have no unique, diagnostic diatom assemblage. Where rapid postseismic sedimentation occurs, our diatom-based transfer function model gives estimates of coseismic deformation that agree with independent estimates of land-level change. Sedimentary hiatuses at two sites following the 2010 earthquake suggest that the magnitude of coseismic deformation may be underestimated in fossil records. Where sediment accumulation allows, criteria for distinguishing between seismic and non-seismic stratigraphies based on evidence for the largest plate boundary earthquakes are corroborated by the lesser magnitude earthquake of 2010. The key to reconstructing earthquake characteristics, such as rupture magnitude and differences between plate-boundary and upper plate sources, depends on applying explicit stratigraphic assessment criteria at multiple sites in order to identify the spatial pattern of deformation associated with each earthquake.

1. Introduction

The Chilean megathrust creates great earthquakes exceeding moment magnitude (M_w) 8, including the greatest magnitude ever recorded, the 1960 M_w 9.5 rupture of the Valdivia segment, and the M_w 8.8 Maule earthquake of 27th February 2010. These earthquakes are characterised by intense, long duration shaking, significant land surface deformation, generation of near-field tsunamis along the Chilean coast and may spawn destructive trans-Pacific tsunamis. Paleoseismic research at other subduction zones suggests historical and instrumental records may be too short to adequately assess the recurrence of the greatest magnitude seismic hazards, a factor contributing to inadequate anticipation of the 2004 Sumatra-Andaman and 2011 Tohoku megathrust earthquakes (Stein and Okal, 2011). Records kept by Spanish settlers and visiting Europeans indicate four megathrust earthquakes in the Valdivia segment over the last 500 years but current paleoseismic evidence records only some of these. Using evidence from tidal marshes, Cisternas et al. (2005) propose a 300-year recurrence interval between the largest ruptures, with the megathrust remaining partly loaded with accumulated plate motion through smaller intervening earthquakes. Differences between the historical and paleoseismic evidence may reflect variations in the size of the rupture zones of megathrust earthquakes; alternatively, interseismic land uplift may lead to low sediment accumulation or erosion of tidal marshes so the sediments record only a partial chronology of great earthquakes. Given the range of processes that may control the preservation of paleoseismic evidence (McCalpin and Carver, 2009), we require correlation of evidence from multiple sites in order to reconstruct the dimensions of land surface deformation and therefore estimate the extent of the segment rupture for each event (Nelson et al., 1996; Atwater and Hemphill-Haley, 1997; Atwater et al., 2005). Analysis of the sedimentary record of the 1960 and 2010 earthquakes provides potential modern analogues for building century to millennial scale paleoseismic records for different segments of the Chilean megathrust.

* Corresponding author. Tel.: +44 (0)191 334 1954.
E-mail addresses: edmund.garrett@durham.ac.uk, edgarrett@gmail.com (E. Garrett).
[1] Current address: Northumbria University, School of the Built and Natural Environment, Ellison Building, Newcastle-upon-Tyne NE1 8ST, UK.

0277-3791/$ – see front matter © 2013 The Authors. Published by Elsevier Ltd. All rights reserved.
http://dx.doi.org/10.1016/j.quascirev.2013.04.007

Following both the 1960 and 2010 earthquakes, measurements of the displacement of coastal landforms and biotic environments, such as shore platforms and intertidal encrusting molluscs, provided the first quantitative maps of coseismic land uplift and subsidence, essential for constraining models of slip distribution (Plafker and Savage, 1970; Moreno et al., 2009; Farías et al., 2010; Lorito et al., 2011; Vargas et al., 2011; Melnick et al., 2012). Such records can be fragmentary in both space and time and sedimentary records from tidal marshes can significantly enhance the paleoseismic record of both the coseismic deformation and changes through complete earthquake deformation cycles (Hamilton and Shennan, 2005). In this paper we aim to develop quantitative reconstructions of relative land surface deformation during the 1960 and 2010 earthquakes based on lithostratigraphy and diatom assemblages from five sites. We compare our results with other estimates of coseismic deformation and use our findings to test the applicability of criteria developed in studies of the Cascadia subduction zone to differentiate between sedimentary evidence of relative land- and sea-level changes of seismic and non-seismic origins (Nelson et al., 1996). The Cascadia studies, from Atwater's (1987) seminal paper onwards, made comparisons with the 1960 Chilean earthquake and the 1964 M_w 9.2 earthquake in Alaska. Nelson et al. (1996) suggested their criteria would apply to magnitude 8 + earthquakes and the 2010 M_w 8.8 Maule earthquake provides the opportunity to directly test them. Finally, we assess the application and limitations of stratigraphic and microfossil approaches for developing Holocene records of multiple earthquake deformation cycles in Chile.

2. Study area and methods

In August 2010, six months after the 27th February Maule earthquake, we completed field investigations of tidal marshes at five sites, which we number from north to south for ease of reference (Fig. 1). Sites 1 and 2 lie in the 2010 segment, sites 3 and 4 in the area where the 1960 and 2010 segments overlap, and site 5 is near the centre of the 1960 segment. The spatial pattern of deformation varies longitudinally within each rupture zone, with distance from the trench controlling the zones of coseismic uplift and subsidence (Fig. 1). We targeted tidal marshes as they may preserve evidence of land-level changes and tsunami inundation in their sediment stratigraphy (Atwater, 1987; Cisternas et al., 2005; Hamilton and Shennan, 2005). We employed transects of pits and short cores across marshes and adjacent coastal lowlands to assess the type, continuity and extent of 2010 tsunami deposition and the lateral extent and net accretion of sediments laid down since the earthquake. Any sub-surface sand layers were also documented and we use local testimony, comparison with other studies and caesium-137 (^{137}Cs) concentrations to suggest which relate to tsunami deposition following the 1960 earthquake.

We selected cores from each transect for further laboratory analyses, including diatom assemblages and grain size variations, to reconstruct relative sea-level changes and to assess the

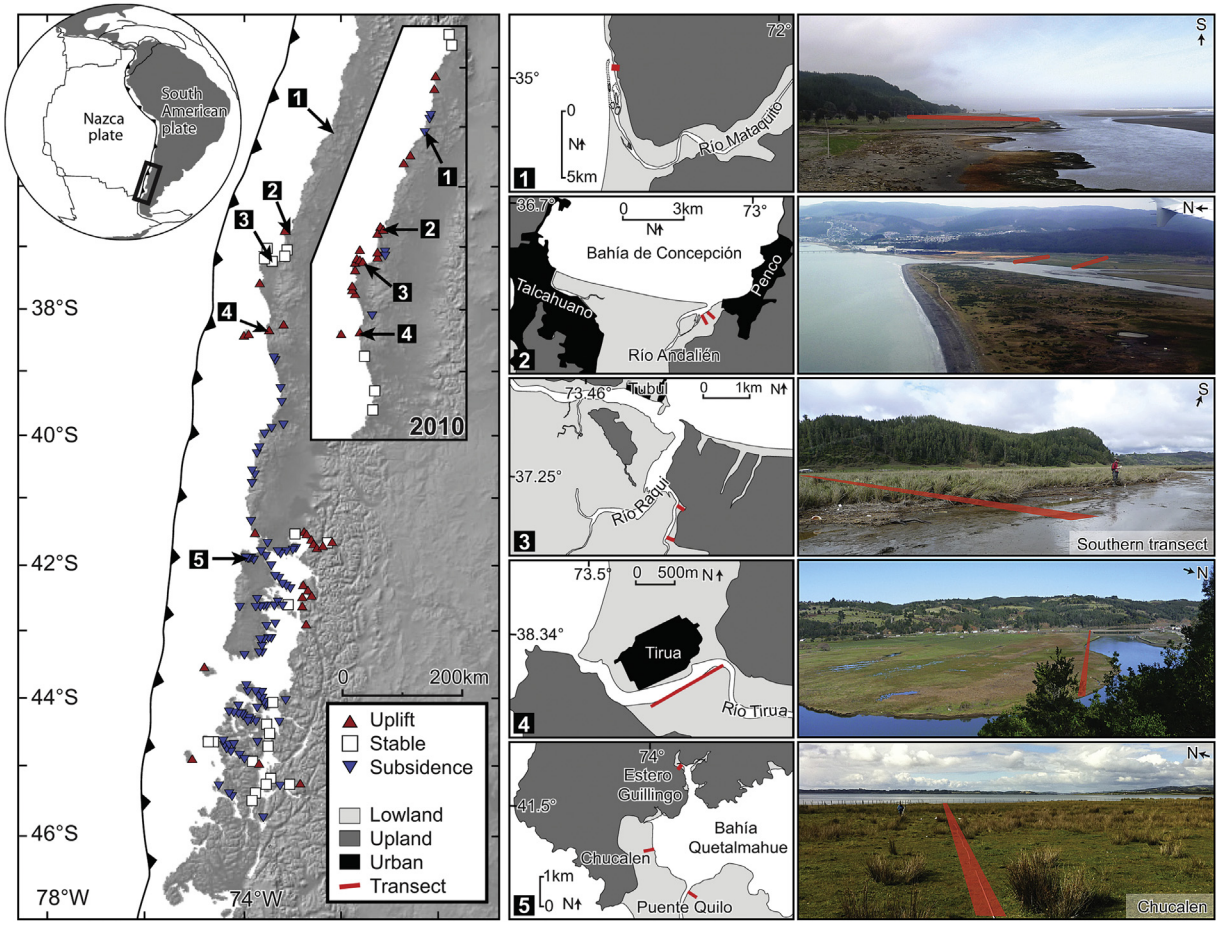

Fig. 1. Tectonic setting of the Chilean subduction zone and the location of the field sites in relation to the 2010 and 1960 rupture zones. Vertical land surface deformation in 1960 (main figure) and 2010 (inset) from Plafker and Savage (1970) and Vargas et al. (2011) respectively. Site 1: Río Mataquito; site 2: Río Andalién; site 3: Tubul; site 4: Río Tirua; site 5: Northern Isla de Chiloé, including Chucalen and the modern transects at Estero Guillingo and Puente Quilo.

composition of tsunami deposits. Laboratory preparation of diatoms followed standard methods (Palmer and Abbott, 1986) with a minimum of 250 diatom valves counted per sample. Diatoms live at the sediment surface (epipelic or epipsammic), attached to vegetation (epiphytic) or in the water column (planktonic) and respond to variations in their environment, including salinity and frequency of tidal inundation (e.g. Vos and de Wolf, 1993). Diatoms may provide information on the depositional environment and source of sediments to a coastal area, for example they can be used to distinguish tsunami deposits from other sediments and help identify the source of tsunami lain sand (Dawson et al., 1996; Hemphill-Haley, 1996; Dawson, 2007; Horton et al., 2011).

Diatom assemblages can also provide estimates of coseismic land movement with decimetre precision (e.g. Shennan et al., 1996; Zong et al., 2003; Hamilton and Shennan, 2005). We estimate coseismic deformation for each site by comparing the diatom assemblages from sediments deposited before and after the earthquake with the modern distribution of diatoms at two tidal marshes in northern Isla de Chiloé, site 5, and data collected by Nelson et al. (2009). We use modern diatom samples collected in 2010 from site 5 only as it was not affected by elevation change or tsunami inundation in 2010. To account for variations in tidal ranges between sites, we convert the elevation of each modern sample to a standardized water level index (SWLI), whereby a SWLI value of 100 represents mean sea level and 200 represents mean higher high water (Hamilton and Shennan, 2005). We define:

$$\mathrm{SWLI}_n = \frac{100(h_n - h_{\mathrm{MSL}})}{h_{\mathrm{MHHW}} - h_{\mathrm{MSL}}} + 100 \quad (1)$$

where:

SWLI_n is the standardised water level index for sample n
h_n is the elevation of sample n
h_{MSL} is Mean Sea Level at the site
h_{MHHW} is Mean Higher High Water at the site

We follow the transfer function approach outlined by Hamilton and Shennan (2005), first using detrended canonical correspondence analysis (DCCA) to determine the requirement for a unimodal method, then developing a transfer function model that can produce reconstructions of marsh surface elevations, with error terms, from fossil diatom sequences (Software: C2 version 1.7.2, Juggins, 2011). Estimates of coseismic deformation compare pre- and post-earthquake marsh surface elevations, accounting for the thickness of any tsunami deposit. We define the uncertainty for each estimate of coseismic deformation:

$$\mathrm{CD\ error} = \sqrt{(E_{\mathrm{PRE}}\ \mathrm{error})^2 + (E_{\mathrm{POST}}\ \mathrm{error})^2} \quad (2)$$

where:

CD error is the 1σ error of the coseismic deformation estimate
E_{PRE} error and E_{POST} error are the sample specific standard errors for samples preceding and following the deformation event respectively.

3. Transfer function model development

The modern training set comprises 96 samples collected in 2010 and 32 collected by Nelson et al. (2009) in 1989 (Supplementary table A.1). DCCA confirms a unimodal relationship between modern diatom distributions and elevation (environmental gradient >2 standard deviations, Birks, 1995) and we use weighted averaging partial least squares regression (WA-PLS) with bootstrapping cross-validation (ter Braak and Juggins, 1993; Birks, 1995). We chose the three-component model over one and two-component models, as it has the highest r^2 value, a more linear distribution of observed against predicted values and a RMSEP improvement of at least 5% with the addition of each extra component (Fig. 2). Increased precision can be obtained by reducing the range of sampled elevations; however we currently have no independent measure to select a model using a narrower elevation range, as applied in Alaska where the data set is more than twice the size (Hamilton and Shennan, 2005).

Given the distance between sites and their different environmental conditions, we may not expect the modern training set to fully reflect the range of diatom assemblages and environments that exist in fossil samples, even though the number of samples exceeds the minimum required to give sample-specific error terms in WA-PLS. We use an analogue measure, modern analogue technique (MAT) to quantify the similarity between each fossil sample and the modern training set using a squared chord distance dissimilarity method (Birks, 1995). We use the 5th percentile of the dissimilarity values for the modern samples as the threshold between a 'good' and 'close' modern analogues for each fossil sample and the 20th percentile as the cut-off for a 'poor' modern analogue.

4. Results and reconstructions of deformation

4.1. Site 1: Río Mataquito

The site lies within the 2010 segment and north of the 1960 segment (Fig. 1). The Río Mataquito is deflected northwards by an 8 km long supratidal sand spit at its confluence with the Pacific. The spit was largely submerged following coseismic deformation in 2010 or eroded by the ensuing tsunami which crested 11 m above tide level (Fig. 3; Vargas et al., 2011). Our transect of short cores from a tidal marsh close to the pre-earthquake river mouth shows the 2010 tsunami deposit to be of variable thickness. The grey sand sheet exceeds 0.4 m in thickness close to the river

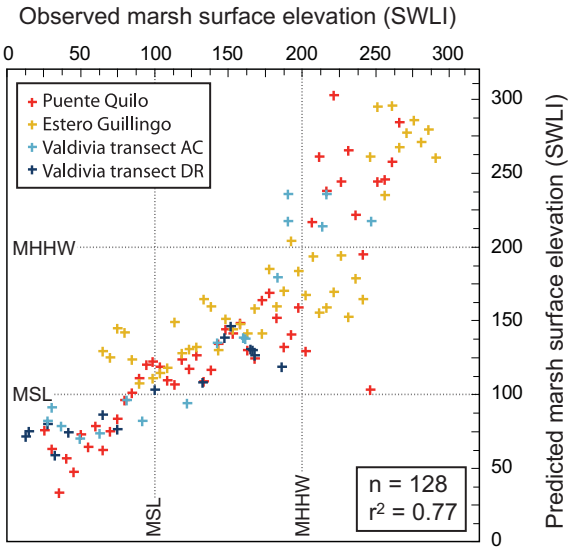

Fig. 2. Observed against predicted elevation values for the four transects included in the WA-PLS component 3 transfer function model. Valdivia AC: samples collected from a fan bordering Río Angachilla; Valdivia transect DR: samples collected from Isla del Rey (Nelson et al., 2009).

Fig. 3. Comparison of pre and post 2010 Maule earthquake Google Earth imagery for sites 1–4. Red lines indicate August 2010 sampling transects. (For interpretation of the references to colour in this figure legend, the reader is referred to the web version of this article.)

channel, and thins in a landward direction (Fig. 4). The lower contact is abrupt, with occasional above ground parts of terrestrial plants preserved immediately beneath and within the sand, pointing in the direction of flow as they were flattened by tsunami inundation. The deposit is normally graded and is both coarser grained and less organic than the underlying tidal marsh sediments.

Diatom assemblages from the tsunami deposit are characterised by epipelic and epipsammic taxa, with a significant minority, ~30%, of planktonic forms (Fig. 5). Almost 65% of the tsunami assemblage is characterised by diatom species identified by the transfer function model as reflecting environments above mean higher high water. A further 25% of the assemblage consists of species not encountered in the modern tidal marshes, with the remaining 10% corresponding to species indicative of environments below mean higher high water.

Despite an increase in accommodation space resulting from the reported coseismic subsidence, (Vargas et al., 2011; Vigny et al., 2011), we do not record any post-tsunami sediment accumulation in the six month interval between the earthquake and field sampling and, therefore, no estimate of coseismic deformation is possible using the diatom-based transfer function.

4.2. Site 2: Río Andalién

The site lies within the 2010 segment and immediately north of the 1960 segment (Fig. 1). Tidal marshes occupy the broad north-facing embayment of the Bahía de Concepción between Talcahuano and Penco. Estimates of coseismic movement in 2010 indicate uplift to the west (Fritz et al., 2011) and subsidence to the south (Vigny et al., 2011). Watermarks in Talcahuano and Penco indicate 2010 tsunami flow depths of between 4 and 7 m (Fritz et al., 2011) and a maximum inundation distance across the low lying tidal marshes of 2.6 km (Morton et al., 2011). We investigated two transects from the eastern edge of the embayment, alongside the Río Andalién (Fig. 2).

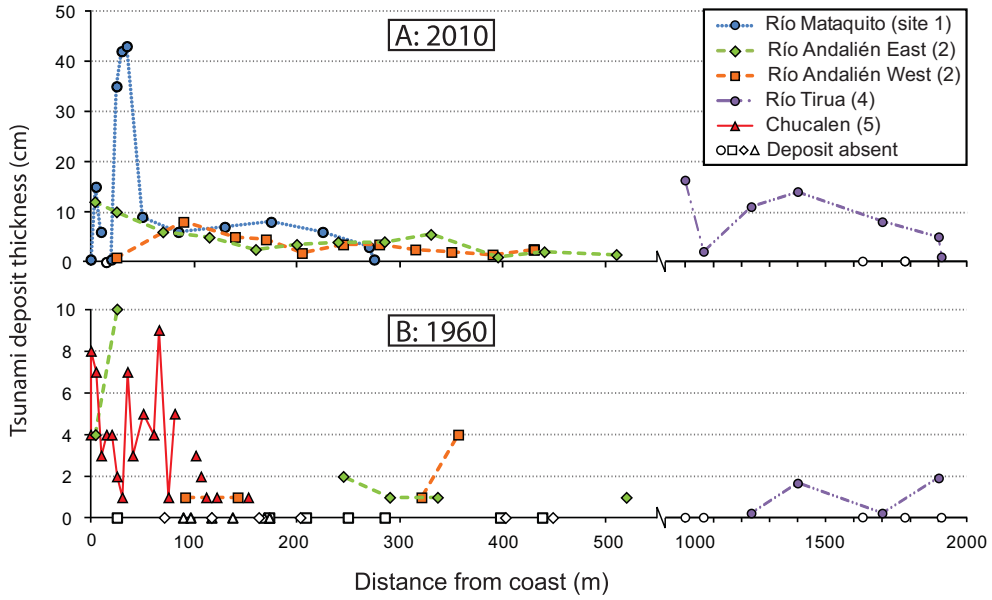

Fig. 4. Thickness, extent and continuity of the 2010 and 1960 tsunami deposits at Río Mataquito, Río Andalién, Río Tirua and Chucalen. We could not locate 2010 tsunami deposits at site 3, Tubul, or site 5, Chucalen. The 1960 tsunami deposit was not identified at site 1, Río Mataquito, or site 3, Tubul. Tsunami deposits may extend further inland than the sampled locations; we did not sample to the limit of inundation. Sampling commenced 1 km inland from the coastline at site 4, Río Tirua, due to the location of tidal marshes at this site. Note the change in *y*-axis scale.

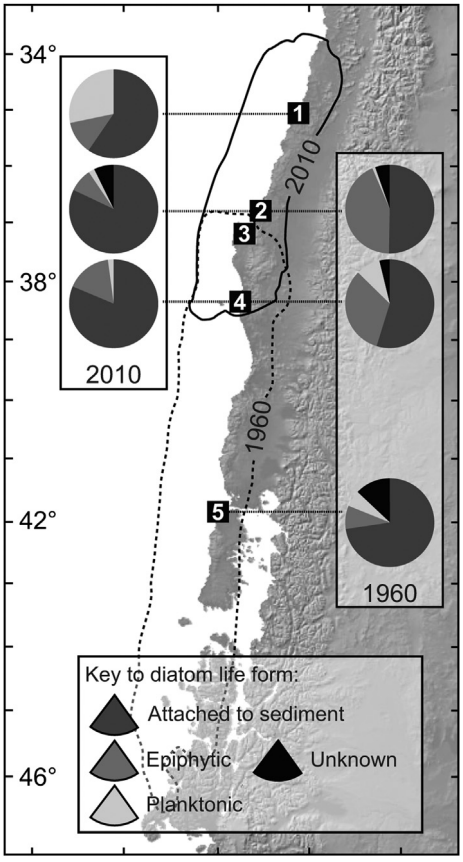

Fig. 5. Diatom assemblages of the 2010 and 1960 tsunami deposits, summarised by life form (following Denys, 1991; Stoermer, 1980; Van Dam et al., 1994; Vos and de Wolf, 1993, 1988). Epipelic and epipsammic species are grouped as *"attached to sediment"*. We do not report any tsunami deposit from site 3, Tubul.

4.2.1. 2010 Earthquake and tsunami

The 2010 tsunami deposit is a largely continuous sand sheet with occasional rounded mud rip-up clasts. The normally graded deposit is generally less than 0.1 m thick and both transects exhibit landward thinning (Fig. 4). The lower boundary is abrupt, however vegetation was generally found to have remained in growth position, rather than having been flattened beneath the sand layer. Diatoms that live attached to sediment account for more than 75% of the 2010 tsunami assemblage (Fig. 5). The summary assemblages (Fig. 6A) show that the tsunami deposit has a greater proportion of species indicative of lower elevations than the underlying tidal marsh sediment, reflecting net sediment transport from the lower intertidal and perhaps subtidal zone during the tsunami.

Six months after the earthquake, postseismic sediment accumulation had reached a maximum of 20 mm. Pre- and post-tsunami diatom assemblages indicate subsidence of 0.75 ± 0.43 m (Fig. 6A), but we note the poor modern analogues and discuss this further in Section 5.3.

4.2.2. 1960 Earthquake and tsunami

A second sand layer occurs approximately 0.2 m below the present ground surface (Fig. 4). Comparison of the colour, grain size and nature of the lower contact with the 2010 tsunami deposit suggests that this lower sand layer was also deposited by a tsunami. Numerous significant tsunamis have struck the coast of central Chile, including major events in 1960, 1835, 1751, 1730, 1657, 1575 and 1570 (Lomnitz, 2004; Cisternas et al., 2005). Tide gauge data from Talcahuano indicate that the 1960 tsunami reached heights of 3 m within Bahía de Concepción (Sievers et al., 1963). Comparable tide gauge measurements of the 2010 tsunami were approximately 0.65 m lower, suggesting that the 1960 tsunami was also of sufficient size to erode, transport and deposit intertidal sediments within the bay. We find elevated ^{137}Cs concentrations immediately below the sand layer; this indicates deposition no earlier than the beginning of atmospheric nuclear testing in 1952, suggesting that the sand layer was deposited in 1960.

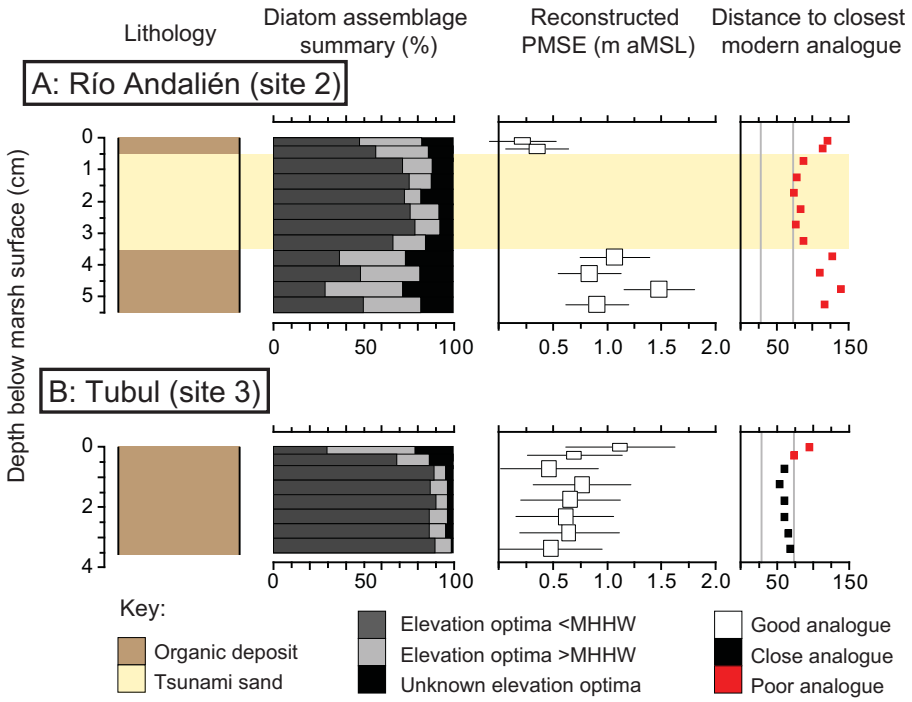

Fig. 6. 2010 Diatom assemblages and paleomarsh surface elevation reconstructions at A: site 2, Río Andalién and B: site 3, Tubul. Due to a lack of post-earthquake sedimentation, reconstructions are not possible for site 1, Río Mataquito, and site 4, Río Tirua. Assemblage summary based on modern species coefficients derived from the WA-PLS transfer function model. We use the distance to the closest modern analogue from the modern analogue technique in C2 (Juggins, 2011) to assess the similarity between modern and fossil assemblages.

Diatom assemblages from this deposit are highly mixed, with epiphytic species and those that live attached to sediment contributing the majority of the assemblage (Fig. 5). Planktonic species are rare, accounting for less than 5% of the assemblage. Species indicative of elevation classes above and below mean higher high water occur approximately equally (Fig. 7A), giving no clear indication of predominant sediment source.

Pre- and post-tsunami diatom assemblages are generally similar, with the largest changes in species that are not characterised by our modern assemblage data (Fig. 7A). Quantitative reconstructions indicate uplift of 0.11 ± 0.45 m, again noting the poor modern analogue classifications.

4.3. Site 3: Tubul

Tubul lies in the area where the 2010 and 1960 segments overlap (Fig. 1). The Tubul and Raqui rivers drain a substantial sheltered tidal and freshwater marsh on the northern edge of the Arauco Peninsula (Figs. 1 and 3). Estimates of coseismic movement in 2010 indicate uplift of between 1 and 2 m (e.g. Farías et al., 2010; Melnick et al., 2012). Our coring transects ranged from intertidal mud and sand flat to freshwater marsh above the influence of tides.

4.3.1. 2010 Earthquake and tsunami

Despite tsunami flow depths estimated at over 5 m (Fritz et al., 2011), we did not observe a surficial or sub-surface tsunami deposit at any location on our transects. This may reflect local effects of coseismic uplift reducing the potential tsunami inundation distance inland and the position of our sampling area with respect to the open coast.

Although we noted no change in sediment lithology in the field, laboratory analysis of the uppermost 5 mm of the recovered sediment profile shows a significant change in diatom assemblage (Fig. 6B). Our reconstruction indicates coseismic uplift of 0.64 ± 0.67 m, with close modern analogues for the pre-earthquake samples.

4.4. Site 4: Río Tirua

The Río Tirua meanders through a low-lying coastal plain, characterised by tidal and freshwater marsh environments. The site is close to the southern limit of surface deformation in 2010 and within the 1960 segment (Fig. 1). Intertidal mussels indicate coseismic uplift of between 0.5 and 1 m in 2010 (Melnick et al., 2012). Our transect lies ~1 km from the open coast (Fig. 3).

4.4.1. 2010 Earthquake and tsunami

While tsunami runup reached 20 m on the exposed rocky shoreline to the southwest, heights closer to the river mouth were approximately half as large (Fritz et al., 2011; Vargas et al., 2011; Bahlburg and Spiske, 2012). The 2010 tsunami deposited a grey sand layer which we traced along the incised banks of the Río Tirua. The deposit exceeds 0.1 m in thickness and thins upstream and, more rapidly, away from the river channel (Fig. 4). The lower contact is abrupt, with frequent flattened stems below and encased within the base of the deposit.

The tsunami diatom assemblage is predominately composed of species that live attached to sediment, with some epiphytic forms (Fig. 5). Taxa favouring the lower elevations of the modern transects contribute 25–45% of the assemblage, with species not found in the modern marshes providing a further 30%.

There was no identifiable postseismic sedimentation six months after the 2010 earthquake. Tsunami-lain sand was still visible at the surface in January 2012, almost two years after the earthquake. No estimate of coseismic deformation is possible using the diatom-based transfer function.

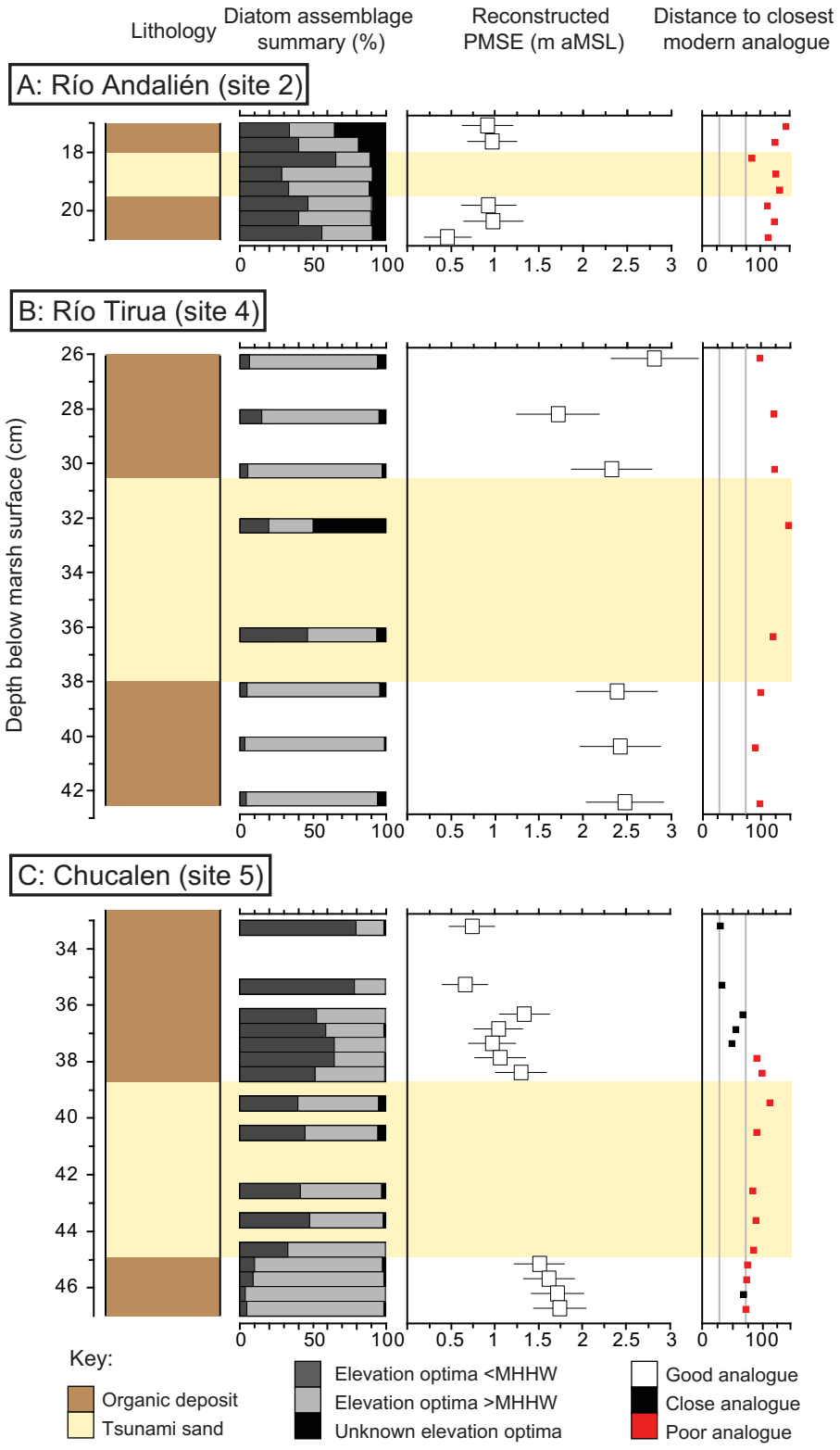

Fig. 7. 1960 Diatom assemblages and paleomarsh surface elevation reconstructions at A: site 2, Río Andalién; B: site 4, Río Tirua and C: site 5, Chucalen. No pre-2010 tsunami deposits were identified at site 1, Río Mataquito, or site 3, Tubul. Assemblage summary based on modern species coefficients derived from the WA-PLS transfer function model. We use the distance to the closest modern analogue from the modern analogue technique in C2 (Juggins, 2011) to assess the similarity between modern and fossil assemblages.

4.4.2. 1960 Earthquake and tsunami

We observed a second sand layer, analogous to that deposited by the 2010 tsunami, at a depth varying between 0.1 and 0.4 m alongside the Río Tirua. The contact with underlying marsh sediments is abrupt. Elevated ^{137}Cs concentrations in the buried marsh surface and the testimony of local residents who experienced the event suggest that this layer relates to the tsunami associated with the 1960 earthquake. Tsunami runup on Isla

Mocha, 30 km offshore from the mouth of the Río Tirua, exceeded 15 m (Sievers et al., 1963), but the wave height as it approached the mainland in this sector is unknown. By way of comparison, runup during 2010 exceeded 20 m on Isla Mocha (Fritz et al., 2011); however the difference may result from the different approach directions of the two tsunamis. The 1960 tsunami deposit is generally thinner and more fragmented than the 2010 deposit (Fig. 4), as we also noted for site 2, Río Andalién.

The 1960 sand layer is characterised by a higher proportion of epiphytic and planktonic species than the 2010 deposit, although epipelic and epipsammic species still contribute more than half of the total assemblage (Fig. 5). Species indicative of elevations above mean higher high water are dominant in most of the tsunami samples; however a peak in the abundance of one species results in almost 50% of one sample consisting of diatoms of unknown elevation preference (Fig. 7B).

Pre- and post-tsunami diatom assemblages are generally similar; however there are no close modern analogues for any of the samples. Our marsh surface reconstructions are indistinguishable from zero, 0.03 ± 0.72 m (Fig. 7B).

4.5. Site 5: Chucalen

On the north west of Isla de Chiloé, tidal marshes line the western fringe of Bahía Quetalmahue, sheltered from the Pacific Ocean by the Lacui Peninsula (Fig. 1). This region is close to the centre of the 1960 segment and ~400 km south of the 2010 segment. There was no tsunami recorded here in 2010.

4.5.1. 1960 Earthquake and tsunami

At Chucalen we traced a grey sandy deposit through a 100 m long transect at depths of between 0.1 and 0.35 m below the present marsh surface (Fig. 4). The normally graded deposit decreases in thickness with increasing elevation and distance from the marsh front. The contact with the underlying marsh sediments is abrupt. Through comparison with preliminary investigations by Bartsch-Winkler and Schmoll (1993), ^{137}Cs concentrations and statements from local residents, we correlate this deposit with the 1960 tsunami. Witnesses suggest that a series of three waves resulted in runup exceeding 15 m on exposed headlands on the northern edge of the Lacui Peninsula, with 5 m waves striking Ancud, decreasing to 1.5 m in Bahía Quetalmahue (Sievers et al., 1963). Bartsch-Winkler and Schmoll (1993), however, suggested waves of several times this magnitude may have entered the Quetalmahue estuary across the isthmus that joins the Lacui Peninsula, close to our sampling area.

Diatoms that live attached to sediment account for almost three quarters of the tsunami deposit assemblage at Chucalen, with diatoms of unknown life form making up the second largest component (Fig. 5). When classified by modern distribution, the tsunami deposit exhibits a greater proportion of species indicative of lower elevations than those from the underlying tidal marsh sediment (Fig. 7C).

Diatom assemblages in sediments immediately above and below the tsunami deposit show a change from species characteristic of the highest elevations of modern tidal marshes to taxa more tolerant of regular tidal inundation (Fig. 7C). Paleomarsh surface elevation reconstructions indicate land subsidence of 1.12 ± 0.53 m.

5. Discussion

5.1. Tsunami deposition

The tidal marshes investigated here demonstrate a variable and fragmentary record of tsunamis associated with two great earthquakes in 1960 and 2010. We found no 2010 tsunami deposit at one of the four marshes adjacent to the rupture zone. Where present, it is composed of more than 85% sand and abruptly overlies finer grained, more organic tidal marsh sediments, frequently preserving flattened but still rooted terrestrial plants at their contact. Flattened vegetation assists in determining tsunami flow direction (e.g. Morton et al., 2011). The extent and continuity of the deposit is highly variable. At Río Mataquito, site 1, the sand layer reaches a maximum of 0.40 m in thickness, however accumulations of 0.05–0.15 m are more common both at this site, and at the other sites investigated. Comparable 2010 tsunami deposit thicknesses are reported by Horton et al. (2011) and Morton et al. (2011). At our sites the 2010 deposit fines in a landward direction, reflecting decreasing sediment transport as the wave train moved inland. We attribute further along-transect variability in the thickness of the deposit to variable vegetation cover and pre-tsunami surface topography (Morton et al., 2007).

The 1960 tsunami deposit is preserved as a continuous stratigraphic layer only at Chucalen, site 5, in the central part of the rupture segment. Towards the northern limit of the 1960 segment it is absent from site 3, Tubul and fragmented at site 4, Río Tirua. It is present, though fragmented at site 2, Río Andalién, just north of the segment boundary, and we did not encounter any buried sand layers at site 1. Where present, the deposit is similar to the 2010 tsunami layer: sand-rich and abruptly overlying organic tidal marsh sediment. The thin and fragmentary nature of the deposit, despite the significant size of the 1960 tsunami, may indicate postseismic erosion prior to burial and encasement into the sediment record.

Diatom assemblages from tsunami sand layers vary both between different sites for the same tsunami and between different tsunamis at the same site. There is no unique tsunami diatom assemblage. Rather, the assemblage reflects the local sediment source, with mixed assemblages of different salinity preferences, different life forms and different habitats. Diatom assemblages are likely to be mixed as tsunamis inundate inland areas and erode, transport and redeposit marine, intertidal and non-marine sediments. Similar mixed assemblages including freshwater, brackish and marine species are observed in tsunami deposits at Pichilemu, central Chile, reported by Horton et al. (2011), and are consistent with observations in modern and paleotsunami deposits elsewhere (Hemphill-Haley, 1996; Atwater and Hemphill-Haley, 1997; Tuttle et al., 2004; Dawson, 2007; Sawai et al., 2008).

5.2. Estimating coseismic land-level change

Transfer function models provide estimates of coseismic land surface deformation for two of the five sites in 2010 and three sites in 1960. The lack of post-earthquake sedimentation or the absence of a 1960 tsunami deposit to guide our sampling approach precludes the quantification of deformation at the remaining sites. Despite our reservations based on the lack of good modern analogues, our reconstructions compare favourably with published estimates of coseismic land-level change (Fig. 8). This confirms the potential of using diatom-based transfer function models to quantify coseismic movement from previous great earthquakes in this region. The apparent offset for the 2010 data (Fig. 8) may be the effect of the lack of good modern analogues, but it may also reflect the different measures of coseismic subsidence. The GPS and benchmark relevelling data relate to the vertical movement of rock surfaces, whereas marsh sediments may undergo additional local scale subsidence due to ground shaking and dewatering leading to sediment consolidation. This was observed at numerous locations in Alaska during the 1964 M_w 9.2 earthquake (Plafker, 1969) and the M_w 8.1 and 8.2 earthquakes in 1899 (Plafker and Thatcher, 2008).

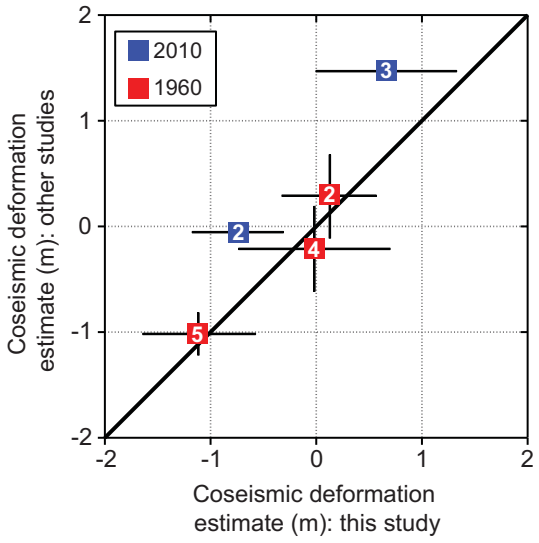

Fig. 8. Comparison of transfer function model estimates of coseismic deformation with published estimates of vertical coseismic deformation in 1960 and 2010 at Río Andalién (2), Tubul (3), Río Tirua (4) and Chucalen (5). Diagonal line is the 1:1 line, not a best-fit regression line. Due to hiatuses or the absence of tsunami deposits, we cannot estimate deformation at sites 1 and 3 for 1960 and at sites 1, 4 and 5 for 2010. For 1960 we compare our estimates with Plafker and Savage's (1970) sampling locations 1, 9 and 45 and for 2010 we compare with the continuous GPS station at Concepción (Vigny et al., 2011) and benchmark relevelling at Tubul (Melnick et al., 2012).

The estimates by Plafker and Savage (1970) for coseismic motions in 1960 may also incorporate some local sediment consolidation, for example their estimate from close to our site 5 based on comparison of the lower growth limit of pre- and post-earthquake vegetation.

5.3. Limitations and improvement of quantitative reconstructions of relative land- and sea-level change

Although the current modern training set includes samples from four transects in two locations and from modern environments ranging from unvegetated tidal flat below mean sea level to above the highest limits of tidal inundation, many of the fossil samples do not have a 'good' or 'close' modern analogue. While this is, in part, a result of our selected percentile thresholds that are stricter than those used in some other studies, the apparent dissimilarity between modern and fossil diatom assemblages remains a cause for concern. We highlight this lack of modern analogues as a limitation of the current study and advocate the need for larger training sets, preferably from a wide range of sites. The modern samples are from locations well to the south of sites 1–4 and there may be a spatial control on diatom assemblages that we are currently unable to assess. Ongoing postseismic deformation and the lack of significant sedimentation preclude the collection and use of samples from sites within the 2010 rupture zone and further investigations should focus on the northern half of the 1960 rupture zone.

Accurate estimates of the magnitude of coseismic deformation depend on the recommencement of sediment accumulation before significant postseismic deformation has occurred. The four marshes in the 2010 rupture zone showed variable responses six months after the earthquake. At site 1, no postseismic sedimentation followed coseismic subsidence and tsunami deposition. Up to 20 mm of sedimentation followed coseismic subsidence and tsunami deposition at site 2. At site 3, up to 5 mm of sedimentation followed coseismic uplift and no tsunami sedimentation and by early 2012, vegetated marsh was developing on previously unvegetated tidal flat. At site 4, no postseismic sedimentation had occurred almost two years after coseismic uplift and tsunami sedimentation in 2010. These postseismic accumulation rates are several orders of magnitude less than after the 1964 Alaskan earthquake (Atwater et al., 2001) and closer to estimates from the channels of the Cruces river following the 1960 Chilean earthquake (Reinhardt et al., 2010). Postseismic vertical movements in the six months following the Maule 2010 earthquake were small, estimated from GPS data at <15 mm at Concepción and <50 mm elsewhere along the rupture zone (Baez et al., 2010). Consequently, postseismic movements are unlikely to significantly affect estimates of coseismic land motions based on sediment biostratigraphy at sites 2 and 3. At sites with a sedimentary hiatus, coseismic deformation estimates will include both coseismic and some postseismic movements, resulting in potential underestimation of the coseismic movement. In fossil sequences it can be very difficult to identify the duration of any hiatus. Radiocarbon dated samples either side of the stratigraphic boundary will give maximum and minimum ages and may identify a large hiatus (e.g. Carver and Plafker, 2008), while reconstructions for the same episode from multiple locations on the same marsh also help (e.g. Shennan and Hamilton, 2006).

5.4. A test of the criteria to differentiate between sedimentary evidence of seismic and non-seismic relative land- and sea-level changes

Based on observations of sedimentary responses to the largest plate boundary earthquakes and similar stratigraphies found in tectonically stable locations, Nelson et al. (1996) propose a series of criteria for differentiating between evidence for seismic and non-seismic relative land- and sea-level changes. Atwater and Hemphill-Haley (1997) apply the same criteria alongside geophysical approaches and structural geology to discuss the differences between plate-boundary and upper-plate sources for the earthquakes, the sizes of the earthquakes, the dimensions of plate-boundary ruptures and the trade-off between size and frequency. Both of these papers point to differences between M_w 7.5 or 8.0 earthquakes and great earthquakes, M_w 8+. The 2010 earthquake provides an opportunity to test the criteria on a smaller plate-boundary rupture than the 1960 Chilean M_w 9.5 and 1964 Alaskan M_w 9.2 earthquakes.

The key criteria outlined by Nelson et al. (1996) are: lateral extent of peat-mud couplets with sharp upper contacts, suddenness of subsidence, amount of subsidence, synchroneity of subsidence with other sites and, for some locations, presence of tsunami sediments. Although these criteria were developed for areas undergoing coseismic subsidence, they are equally applicable to identifying coseismic uplift (Shennan et al., 2009). Section 5.1, above, demonstrates the variable pattern of tsunami deposition, but confirms that, where present, it is a valuable line of evidence and may occur in either uplifted or subsided locations. Our work on the 2010 earthquake deposits suggests that, in south central Chile, sedimentary hiatuses and low rates of sedimentation may temporarily postpone the formation of the characteristic subsidence stratigraphy (Section 5.2), but the burial and preservation of the 1960 deposits shows that any hiatus is brief in the context of multiple earthquake cycles. Our diatom-based reconstructions of relative land/sea-level change are promising, but require a greater range of modern samples in order to provide better modern analogues and greater confidence in the elevation estimates and associated error terms. Nelson et al. (1996) and Atwater and Hemphill-Haley (1997) draw attention to a lower limit of resolution for identifying coseismic deformation; approximately 0.5 m. Our estimates, Section 5.2, currently do not suggest any finer

resolution. Comparison of the marsh sediment sequences for the 2010 and 1960 earthquakes suggests that they produce similar stratigraphic records and that the key to reconstructing earthquake characteristics, such as the rupture magnitude and differences between plate-boundary and upper-plate sources, depends on applying the stratigraphic criteria at multiple sites in order to identify the spatial pattern of deformation associated with each earthquake.

5.5. Implications for reconstructing Holocene megathrust earthquake rupture zones

Precise estimates of coseismic deformation are required from multiple sites to constrain models of the location, dimensions and slip distribution of megathrust earthquakes (Atwater and Hemphill-Haley, 1997; Atwater et al., 2005). To date, elastic deformation models of the 1960 and 2010 earthquakes have been constrained by GPS vectors and measurements of displaced coastal landforms and biotic environments (e.g. Plafker and Savage, 1970; Moreno et al., 2009; Farías et al., 2010; Lorito et al., 2011). Further development of the diatom-based transfer function approach detailed here provides an additional viable method for validating models of these earthquakes, with the added benefit of applicability to older ruptures. Databases of coseismic deformation index points, each characterised by a vertical deformation estimate with an associated error term and spatial and chronological attributes, may be used to assist estimation of the magnitude of historical and prehistoric earthquakes. Such databases have already been successfully employed to constrain the magnitude of past great earthquakes in Cascadia (Atwater and Hemphill-Haley, 1997; Leonard et al., 2004, 2010; Hawkes et al., 2011). The development of this approach along the Chilean subduction zone may allow further investigation of the variability in rupture mode in the 1960 segment (Cisternas et al., 2005) and confirm or refute the permanence of the Arauco Peninsula as a segment boundary over multiple seismic cycles.

Differentiation between the closely temporally spaced rupture of two adjacent segments and a single, multi-segment rupture may prove crucial to interpreting evidence for the largest Holocene megathrust earthquakes (Atwater and Hemphill-Haley, 1997; Atwater et al., 2005; Shennan, 2009; Shennan et al., 2009). While radiocarbon dating alone may be insufficient to distinguish between single and multi-segment ruptures, the work presented here establishes the stratigraphic separation of two closely timed earthquakes in locations close to a seismic segment boundary. We suggest that detailed marsh surface elevation reconstructions from boundary locations, combined with precise dating approaches, should form an integral part of establishing the long-term history of the seismic hazards associated with the Chilean subduction zone.

6. Conclusions

The 1960 and 2010 Chilean great earthquakes provide critical modern analogues for sedimentary processes during seismic cycles at plate boundaries. The major conclusions of this work are:

1) Deposits from the 1960 and 2010 tsunamis are fragmentary, variable and have no unique, diagnostic diatom assemblage.
2) Our transfer function method provides estimates of coseismic land surface deformation for two sites in 2010 and three sites in 1960. Reconstructions agree with independent estimates, confirming the potential for our approach to be used to quantify coseismic deformation for previous great earthquakes in south central Chile.
3) Sedimentary hiatuses at two sites following the 2010 earthquake indicate that the magnitude of coseismic deformation may be underestimated in fossil records.
4) A lack of close modern analogues for fossil diatom assemblages remains a limitation of the current study and we advocate the need for larger training sets, preferably from a wide range of sites.
5) Where sediment accumulation allows, criteria for distinguishing between seismic and non-seismic stratigraphies developed from evidence for the largest plate boundary earthquakes (Nelson et al., 1996; Atwater and Hemphill-Haley, 1997) are corroborated by the lesser magnitude earthquake of 2010.

Acknowledgements

We acknowledge the support of our Chilean colleagues, particularly Marco Cisternas, in getting this research off the ground. A NERC Urgency Grant (I00503X/1) supported a rapid assessment following the 2010 earthquake. EG funded by the Royal Geographical Society (with the Institute of British Geographers), the British Society for Geomorphology and the Quaternary Research Association.

Appendix A. Supplementary data

Supplementary data related to this article can be found at http://dx.doi.org/10.1016/j.quascirev.2013.04.007.

References

Atwater, B.F., 1987. Evidence for great Holocene earthquakes along the outer coast of Washington State. Science 236 (4804), 942–944.
Atwater, B.F., Hemphill-Haley, E., 1997. Recurrence Intervals for Great Earthquakes of the Past 3,500 Years at Northeastern Willapa Bay. U.S. Geological Survey, Washington, p. 108. Professional Paper No. 1576.
Atwater, B.F., Yamaguchi, D.K., Bondevik, S., Barnhardt, W.A., Amidon, L.J., Benson, B.E., Skjerdal, G., Shulene, J.A., Nanayama, F., 2001. Rapid resetting of an estuarine recorder of the 1964 Alaska earthquake. Geological Society of America Bulletin 113 (9), 1193–1204.
Atwater, B.F., Musumi-Rokkaku, S., Satake, K., Tsuji, T., Ueda, K., Yamaguchi, D.K., 2005. The Orphan Tsunami of 1700. Japanese Clues to a Parent Earthquake in North America. U.S. Geological Survey, p. 133. Professional Paper No. 177.
Baez, J., Bataille, K., Tassara, A., Bevis, M.G., Kendrick, E.C., Vigny, C., Brooks, B.A., Smalley, R., Ryder, I.M., Parra, H., Moreno, M., Melnick, D., Barrientos, S.E., Blume, F., 2010. Co- and Post-seismic Surface Deformation Produced by the Maule Earthquake as Observed by a Dense Network of Continuous GPS Stations. Abstract G33A-0838, AGU Fall Meeting, San Francisco.
Bahlburg, H., Spiske, M., 2012. Sedimentology of tsunami inflow and backflow deposits: key differences revealed in a modern example. Sedimentology 59, 1063–1086.
Bartsch-Winkler, S., Schmoll, H., 1993. Evidence for late Holocene relative sea-level fall from reconnaissance stratigraphical studies in an area of earthquake-subsided intertidal deposits, Isla Chiloe, southern Chile. In: Frostwick, L.E., Steel, R.J. (Eds.), Tectonic Controls and Signatures in Sedimentary Successions. Blackwell Publishing Ltd., Oxford, pp. 91–108.
Birks, H.J.B., 1995. Quantitative palaeoenvironmental reconstructions. In: Maddy, D., Brew, J.S. (Eds.), Statistical Modelling of Quaternary Science Data. Quaternary Research Association, London, pp. 161–254.
Carver, G., Plafker, G., 2008. Paleoseismicity and neotectonics of the Aleutian subduction zone – an overview. In: Freymueller, J.T., Haeussler, P.J., Wesson, R., Ekstrom, G. (Eds.), Active Tectonics and Seismic Potential of Alaska. American Geophysical Union Geophysical Monograph Series, vol. 179, p. 350.
Cisternas, M., Atwater, B.F., Torrejon, F., Sawai, Y., Machuca, G., Lagos, M., Eipert, A., Youlton, C., Salgado, I., Kamataki, T., Shishikura, M., Rajendran, C.P., Malik, J.K., Rizal, Y., Husni, M., 2005. Predecessors of the giant 1960 Chile earthquake. Nature 437, 404–407.
Dawson, S., 2007. Diatom biostratigraphy of tsunami deposits: examples from the 1998 Papua New Guinea tsunami. Sedimentary Geology 200 (3–4), 328–335.
Dawson, S., Smith, D.E., Ruffman, A., Shi, S., 1996. The diatom biostratigraphy of tsunami sediments: examples from recent and middle Holocene events. Physics and Chemistry of The Earth 21 (1–2), 87–92.
Denys, L., 1991. A Check-list of the Diatoms in the Holocene Deposits of the Western Belgian Coastal Plain with a Survey of Their Apparent Ecological Requirements. In: I. Introduction, Ecological Code and Complete List, p. 41. Belgische Geologische Dienst, Professional Paper 1991/2, No 246.

Farías, M., Vargas, G., Tassara, A., Carretier, S., Baize, S., Melnick, D., Bataille, K., 2010. Land-level changes produced by the Mw 8.8 2010 Chilean earthquake. Science 329 (5994), 916.
Fritz, H.M., Petroff, C.M., Catalán, P.A., Cienfuegos, R., Winckler, P., Kalligeris, N., Weiss, R., Barrientos, S.E., Meneses, G., Valderas-Bermejo, C., Ebeling, C., Papadopoulos, A., Conteras, M., Almar, R., Dominguez, J.C., Synolakis, C.E., 2011. Field survey of the 27 February 2010 Chile tsunami. Pure and Applied Geophysics 168 (11), 1989–2010.
Hamilton, S., Shennan, I., 2005. Late Holocene relative sea-level changes and the earthquake deformation cycle around upper Cook Inlet, Alaska. Quaternary Science Reviews 24 (12–13), 1479–1498.
Hawkes, A.D., Horton, B.P., Nelson, A.R., Vane, C., Sawai, Y., 2011. Coastal subsidence in Oregon, USA, during the giant Cascadia earthquake of AD 1700. Quaternary Science Reviews 30 (3–4), 364–376.
Hemphill-Haley, E., 1996. Diatoms as an aid in identifying late-Holocene tsunami deposits. The Holocene 6 (4), 439–448.
Horton, B.P., Sawai, Y., Hawkes, A.D., Witter, R.C., 2011. Sedimentology and paleontology of a tsunami deposit accompanying the great Chilean earthquake of February 2010. Marine Micropaleontology 79 (3–4), 132–138.
Juggins, S., 2011. C2 Version 1.7.2: Software for Ecological and Palaeoecological Data Analysis and Visualisation. University of Newcastle, Newcastle upon Tyne.
Leonard, L.J., Hyndman, R.D., Mazzotti, S., 2004. Coseismic subsidence in the 1700 great Cascadia earthquake: coastal estimates versus elastic dislocation models. Geological Society of America Bulletin 116 (5–6), 655–670.
Leonard, L.J., Currie, C.A., Mazzotti, S., Hyndman, R.D., 2010. Rupture area and displacement of past Cascadia great earthquakes from coastal coseismic subsidence. Geological Society of America Bulletin 122 (11–12), 2079–2096.
Lomnitz, C., 2004. Major earthquakes of Chile: a historical survey, 1535–1960. Seismological Research Letters 75 (3), 368–378.
Lorito, S., Romano, F., Atzori, S., Tong, X., Avallone, A., McCloskey, J., Cocco, M., Boschi, E., Piatanesi, A., 2011. Limited overlap between the seismic gap and coseismic slip of the great 2010 Chile earthquake. Nature Geoscience 4, 173–177.
McCalpin, J.P., Carver, G.A., 2009. Paleoseismology of compressional tectonic environments. In: McCalpin, J.P. (Ed.), Paleoseismology. International Geophysics, vol. 95, pp. 315–419.
Melnick, D., Cisternas, M., Moreno, M., Norambuena, R., 2012. Estimating coseismic coastal uplift with an intertidal mussel: calibration for the 2010 Maule Chile earthquake ($M_w = 8.8$). Quaternary Science Reviews 42, 29–42.
Moreno, M.S., Bolte, J., Klotz, J., Melnick, D., 2009. Impact of megathrust geometry on inversion of coseismic slip from geodetic data: application to the 1960 Chile earthquake. Geophysical Research Letters 36 (L16310), 5.
Morton, R.A., Gelfenbaum, G., Jaffe, B.E., 2007. Physical criteria for distinguishing sandy tsunami and storm deposits using modem examples. Sedimentary Geology 200 (3–4), 184–207.
Morton, R.A., Gelfenbaum, G., Buckley, M.L., Richmond, M., 2011. Geological effects and implications of the 2010 tsunami along the central coast of Chile. Sedimentary Geology 242 (1), 34–51.
Nelson, A.R., Shennan, I., Long, A.J., 1996. Identifying coseismic subsidence in tidal-wetland stratigraphic sequences at the Cascadia subduction zone of western North America. Journal of Geophysical Research 101 (B3), 6115–6135.
Nelson, A.R., Kashima, K., Bradley, L.A., 2009. Fragmentary evidence of great-earthquake subsidence during Holocene emergence, Valdivia estuary, south central Chile. Bulletin of the Seismological Society of America 99 (1), 71–86.
Palmer, A.J., Abbott, W.H., 1986. Diatoms as indicators of sea level change. In: Van de Plassche, O. (Ed.), Sea Level Research: a Manual for the Collection and Evaluation of Data. Geobooks, Norwich, pp. 457–488.
Plafker, G., 1969. Tectonics of the March 27, 1964, Alaska Earthquake. U.S. Geological Survey, p. 74. Professional Paper No. 543-I.
Plafker, G., Savage, J.C., 1970. Mechanisms of Chilean earthquakes of May 21 and May 22, 1960. Geological Society of America Bulletin 81 (4), 1001–1030.
Plafker, G., Thatcher, W., 2008. Geological and geophysical evaluation of the mechanisms of the great 1899 Yakutat Bay earthquakes. In: Freymueller, J.T., Haeussler, P.J., Wesson, R., Ekstrom, G. (Eds.), Active Tectonics and Seismic Potential of Alaska. Geophysical Monograph Series, vol. 179. American Geophysical Union, Washington, p. 350.
Reinhardt, E.G., Nairn, R.B., Lopez, G., 2010. Recovery estimates for the Río Cruces after the May 1960 Chilean earthquake. Marine Geology 269 (1–2), 18–33.
Sawai, Y., Fujii, Y., Fujiwara, O., Kamataki, T., Komatsubara, J., Okamura, Y., Satake, K., Shishikura, M., 2008. Marine incursions of the past 1500 years and evidence of tsunamis at Suijin-numa, a coastal lake facing the Japan trench. Holocene 18 (4), 517–528.
Shennan, I., 2009. Late Quaternary sea-level changes and palaeoseismology of the Bering Glacier region, Alaska. Quaternary Science Reviews 28 (17–18), 1762–1773.
Shennan, I., Hamilton, S., 2006. Coseismic and pre-seismic subsidence associated with great earthquakes in Alaska. Quaternary Science Reviews 25, 1–8.
Shennan, I., Long, A.J., Rutherford, M.M., Green, F.M., Innes, J.B., Lloyd, J.M., Zong, Y., Walker, K., 1996. Tidal marsh stratigraphy, sea-level change and large earthquakes, 1; a 5000 year record in Washington, U.S.A. Quaternary Science Reviews 15 (10), 1–37.
Shennan, I., Bruhn, R., Plafker, G., 2009. Multi-segment earthquakes and tsunami potential of the Aleutian megathrust. Quaternary Science Reviews 28 (1–2), 7–13.
Sievers, H.A., Villegas, G., Barros, G., Saint-Amand, P., 1963. The seismic sea wave of 22 May 1960 along the Chilean coast. Bulletin of the Seismological Society of America 53 (6), 1125–1190.
Stein, S., Okal, E.A., 2011. The size of the 2011 Tohoku earthquake need not have been a surprise. Eos Transactions American Geophysical Union 92 (27), 227.
Stoermer, E.F., 1980. Characteristics of Benthic Algal Communities in the Upper Great Lakes, p. 79. United States Environmental Protection Agency Report EPA-600/3-80-073.
ter Braak, C.J.F., Juggins, S., 1993. Weighted averaging partial least squares regression (WA-PLS): an improved method for reconstructing environmental variables from species assemblages. Hydrobiologia 269–270 (1), 485–502.
Tuttle, M.P., Ruffman, A., Anderson, T., Jeter, H., 2004. Distinguishing tsunami from storm deposits in eastern North America: the 1929 Grand Banks tsunami versus the 1991 Halloween storm. Seismological Research Letters 75 (1), 117–131.
Van Dam, H., Mertens, A., Sinkeldam, J., 1994. A coded checklist and ecological indicator values of freshwater diatoms from the Netherlands. Netherlands Journal of Aquatic Ecology 28 (1), 117–133.
Vargas, G., Farías, M., Carretier, S., Tassara, A., Baize, S., Melnick, D., 2011. Coastal uplift and tsunami effects associated to the 2010 Mw 8.8 Maule earthquake in Central Chile. Andean Geology 38 (1), 219–238.
Vigny, C., Socquet, A., Peyrat, S., Ruegg, J.-C., Métois, M., Madariaga, R., Morvan, S., Lancieri, M., Lacassin, R., Campos, J., Carrizo, D., Bejar-Pizarro, M., Barrientos, S., Armijo, R., Aranda, C., Valderas-Bermejo, M.-C., Ortega, I., Bondoux, F., Baize, S., Lyon-Caen, H., Pavez, A., Vilotte, J.P., Bevis, M., Brooks, B., Smalley, R., Parra, H., Baez, J.-C., Blanco, M., Cimbaro, S., Kendrick, E., 2011. The 2010 Mw 8.8 Maule megathrust earthquake of central Chile, monitored by GPS. Science 332 (6036), 1417–1421.
Vos, P.C., de Wolf, H., 1993. Diatoms as a tool for reconstructing sedimentary environments in coastal wetlands; methodological aspects. Hydrobiologia 269–270 (1), 285–296.
Vos, P.C., de Wolf, H., 1988. Methodological aspects of paleo-ecological diatom research in coastal areas of the Netherlands. Geologie en Mijnbouw 67, 31–40.
Zong, Y., Shennan, I., Combellick, R.A., Hamilton, S.L., Rutherford, M.M., 2003. Microfossil evidence for land movements associated with the AD 1964 Alaska earthquake. Holocene 13 (1), 7–20.